



THE UNIVERSITY *of* EDINBURGH

Edinburgh Research Explorer

Summit of the N=40 Island of Inversion: precision mass measurements and ab initio calculations of neutron-rich chromium isotopes

Citation for published version:

Silwal, R, Andreoiu, C, Ashrafkhani, B, Bergmann, J, Brunner, T, Cardona, J, Dietrich, K, Dunling, E, Gwinner, G, Hockenbery, Z, Holt, JD, Izzo, C, Jacobs, A, Javaji, A, Kootte, B, Lan, Y, Lunney, D, Lykiardopoulou, EM, Miyagi, T, Mougeot, M, Mukul, I, Murbock, T, Porter, WS, Reiter, M, Ringuette, J, Dilling, J & Kwiatkowski, AA 2022, 'Summit of the N=40 Island of Inversion: precision mass measurements and ab initio calculations of neutron-rich chromium isotopes', *Physics Letters B*, vol. 833, 137288, pp. 1-7. <https://doi.org/10.1016/j.physletb.2022.137288>

Digital Object Identifier (DOI):

[10.1016/j.physletb.2022.137288](https://doi.org/10.1016/j.physletb.2022.137288)

Link:

[Link to publication record in Edinburgh Research Explorer](#)

Document Version:

Publisher's PDF, also known as Version of record

Published In:

Physics Letters B

General rights

Copyright for the publications made accessible via the Edinburgh Research Explorer is retained by the author(s) and / or other copyright owners and it is a condition of accessing these publications that users recognise and abide by the legal requirements associated with these rights.

Take down policy

The University of Edinburgh has made every reasonable effort to ensure that Edinburgh Research Explorer content complies with UK legislation. If you believe that the public display of this file breaches copyright please contact openaccess@ed.ac.uk providing details, and we will remove access to the work immediately and investigate your claim.





Summit of the N=40 island of inversion: Precision mass measurements and ab initio calculations of neutron-rich chromium isotopes



R. Silwal^{a,b,*}, C. Andreoiu^c, B. Ashrafkhani^d, J. Bergmann^e, T. Brunner^f, J. Cardona^{a,g}, K. Dietrich^{a,h}, E. Dunling^{a,i}, G. Gwinner^g, Z. Hockenbery^{a,f}, J.D. Holt^{a,f}, C. Izzo^a, A. Jacobs^{a,j}, A. Javaji^{a,j}, B. Kootte^{a,g}, Y. Lan^{a,j}, D. Lunney^k, E.M. Lykiardopoulou^{a,j}, T. Miyagi^{a,l,m}, M. Mougeot^{n,o}, I. Mukul^a, T. Murböck^a, W.S. Porter^{a,j}, M. Reiter^p, J. Ringuette^{a,q}, J. Dilling^{a,j}, A.A. Kwiatkowski^{a,r}

^a TRIUMF, Vancouver, BC V6T2A3, Canada

^b Department of Physics and Astronomy, Appalachian State University, Boone, NC 28608, USA

^c Department of Chemistry, Simon Fraser University, Burnaby, BC V5A1S6, Canada

^d Department of Physics and Astronomy, University of Calgary, Calgary, AB T2N 1N4, Canada

^e Physikalisches Institut, Justus-Liebig-Universität, Gießen 35392, Germany

^f Department of Physics, McGill University, Montreal, QC H3A0G4, Canada

^g Department of Physics and Astronomy, University of Manitoba, Winnipeg, MB R3T 2N2, Canada

^h University of Heidelberg, Philosophenweg 12, Heidelberg 69120, Germany

ⁱ Department of Physics, University of York, York YO10 5DD, UK

^j Department of Physics and Astronomy, University of British Columbia, Vancouver, BC V6T 1Z4, Canada

^k Université Paris-Saclay, IJCLab-IN2P3/CNRS, France

^l Technische Universität Darmstadt, Department of Physics, Darmstadt 64289, Germany

^m ExtreMe Matter Institute EMMI, GSI Helmholtzzentrum für Schwerionenforschung GmbH, Darmstadt 64291, Germany

ⁿ CERN, 1211 Geneva 23, Switzerland

^o Max-Planck-Institut für Kernphysik, Heidelberg 69117, Germany

^p School of Physics and Astronomy, University of Edinburgh, Edinburgh EH8 9YL, UK

^q Department of Physics, Colorado School of Mines, Golden, CO 80401, USA

^r Department of Physics and Astronomy, University of Victoria, Victoria, BC V8P 5C2, Canada

ARTICLE INFO

Article history:

Received 23 December 2021

Received in revised form 18 April 2022

Accepted 5 July 2022

Available online 12 July 2022

Editor: D.F. Geesaman

Keywords:

Mass measurement

MR-TOF-MS

Nuclear structure

Two neutron separation energies

Island of inversion

Intruder configuration

ABSTRACT

Mass measurements continue to provide invaluable information for elucidating nuclear structure and scenarios of astrophysical interest. The transition region between the $Z = 20$ and 28 proton shell closures is particularly interesting due to the onset and evolution of nuclear deformation as nuclei become more neutron-rich. This provides a critical testing ground for emerging ab-initio nuclear structure models. Here, we present high-precision mass measurements of neutron-rich chromium isotopes using the sensitive electrostatic Multiple-Reflection Time-Of-Flight Mass Spectrometer (MR-TOF-MS) at TRIUMF's Ion Trap for Atomic and Nuclear Science (TITAN) facility. Our high-precision mass measurements of $^{59,61-63}\text{Cr}$ confirm previous results, and the improved precision in measurements of $^{64-65}\text{Cr}$ refine the mass surface beyond $N=40$. With the ab initio in-medium similarity renormalization group, we examine the trends in collectivity in chromium isotopes and give a complete picture of the $N=40$ island of inversion from calcium to nickel.

© 2022 The Author(s). Published by Elsevier B.V. This is an open access article under the CC BY license (<http://creativecommons.org/licenses/by/4.0/>). Funded by SCOAP³.

1. Introduction

Mass measurements are essential to derive the binding energy of the nucleus needed to understand the nuclear forces that hold

the nucleons together [1], and constrain nuclear reaction rates. Such measurements for radioactive nuclei play an important role to enhance our knowledge of nuclear structure, for instance, via the study of evolution of magicity in the nuclear chart. New contenders of nuclei with magic behavior (typically associated with shell gaps in the mass surface, large $2+$ excitation energies, reduced transition probabilities, among others) were discovered from measurements of nuclei far from stability [2,3]. Magic behavior has

* Corresponding author.

E-mail address: silwal@appstate.edu (R. Silwal).

also been reported for $^{52,54}\text{Ca}$ ($Z=20$, $N=32, 34$) [4,5] and ^{68}Ni ($Z=28$, $N=40$) [6] with relatively weak sub-shell closures. Complementing new areas of magicity are regions where expected magic behavior breaks down [2,3]. One example is the $N=20$ islands of inversion (IOI), originally discovered through mass measurements [3,7], followed by the $N=28$ IOI [8,9]. Beyond $N=28$, the $N=40$ region has gathered much interest in the last decade as a possible IOI site with signs of strong collective behavior and shape deformation [10–17]. Some measurements suggest the collective behavior to persist even past $N=40$ isotones [18,19], and with large-scale shell-model calculations predicting even an extension to a fifth IOI [20,21]. Since such an IOI is currently beyond reach of experiment, this prediction should be checked by other theoretical approaches. Therefore, further refining the current ab-initio theories is essential to better describe the changing shell structure.

For exotic nuclei with a large asymmetry in their proton-neutron ratios, the existing mean-field picture deviates drastically when extrapolated to unmeasured isotopes. These are sometimes attributed to the tensor forces arising from the nucleon-nucleon interactions that shift the single-particle energies in the proton/neutron orbitals [22] creating an IOI. The neutron-rich Cr ($Z=24$, $N=40$) isotopic chain that lies midway between the proton shell closures Ca ($Z=20$) and Ni ($Z=28$) region is particularly interesting given its extreme proton-neutron ratios. When protons are added to the $1f_{7/2}$ orbital, the relative energies of the neutron $2p_{1/2,3/2}$ and $1f_{5/2}$ orbitals change due to the strong attractive spin-flip interaction between the proton and neutron orbitals. The change in the energy gap between the pf orbitals leads to rapid changes in collectivity for nuclides along the $N=40$ isotones. Intruder states in such cases can even become ground states due to strong quadrupole deformation, hence implying an IOI around $N=40$ for Fe and Cr isotopes [18,23], similar to the $N=20$ IOI in Mg [24].

A recent precision mass measurement [15] shows a gradual enhancement of collective behavior in Cr isotopes indicated by the flattening of the two-neutron separation energies up to $N=39$. However, calculations with the Universal nuclear energy-density functional (UNEDF0) interaction [25] performed for comparison predict a spherical ^{64}Cr ($N=40$) ground state with an onset of deformation beginning only at ^{68}Cr ($N=44$). Santamaria *et al.* [18] presents a similar flat behavior of the E_{2+} energies from $N=38$ to $N=42$ for Cr isotopes. Their work suggests the maximum collectivity has not been reached at ^{66}Cr and shows the need for further measurements to elucidate the extension from $N=40$ IOI to $N=50$ isotones. A new calculated level scheme for $^{62,64}\text{Cr}$ beyond the (4_1^+) state with γ -ray spectroscopy was recently proposed [10]. Their work predicts collective structures for these isotopes and argues ^{62}Cr to be a transitional system to the path to maximal collectivity of the $N=40$ IOI.

Here, we present results from precise measurements of $^{59,61-65}\text{Cr}$ with a Multiple-Reflection Time-of-Flight Mass Spectrometer (MR-TOF-MS), including the first high-precision direct mass measurements of $^{64,65}\text{Cr}$. Our mass measurement of $^{64,65}\text{Cr}$ extends the mass trend of chromium isotopes and sheds light on how the collectivity evolves in this mass region with their comparison to new results from state-of-the-art ab-initio valence-space in-medium similarity renormalization group (VS-IMSRG) calculations [26], with which we explore the entire $N=40$ island of inversion region from calcium to nickel.

2. Experiment

The mass measurements for $^{59,61-65}\text{Cr}$ were performed with the MR-TOF-MS [27], part of the TITAN facility shown in Fig. 1. A 480 MeV, 15 μA proton beam was impinged upon a UC_X target at the Isotope Separator and Accelerator (ISAC) facility [28]. The el-

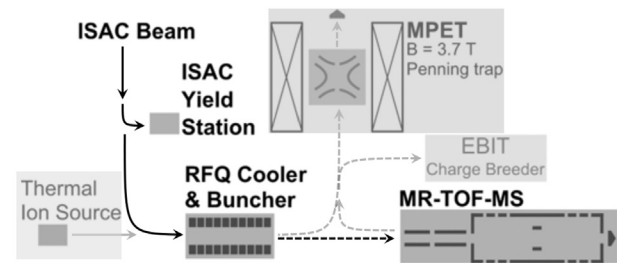


Fig. 1. A schematic diagram of TITAN showing various ion traps. The MR-TOF-MS was used during the measurements and the traps that were not used are shaded in gray.

ement of interest ^{24}Cr along with few contaminant atomic species and diatomic oxide and fluoride molecules were surface ionized by a heated Re surface ion source. The ionization of ^{24}Cr was enhanced using a two-step resonant ionization laser scheme by the TRIUMF Resonant Ionization Laser Ion Source (TRILIS) [29,30].

The resulting beam was then reduced to a single mass unit using the ISAC dipole magnetic separator [31] and was transported to the Radio-Frequency Quadrupole (RFQ) cooler & buncher [32] at the TITAN facility. Here, it was bunched and cooled for 20 ms by collisions with He buffer gas. The cooled radioactive beam was then sent to the TITAN MR-TOF-MS [27] for mass measurements.

Details of the operation and performance of the TITAN MR-TOF-MS are summarized in [33]. The device is based on the MR-TOF-MS in operation at the FRS Ion Catcher [34]. Inside the MR-TOF-MS, the ion bunches were transported to a dedicated injection trap, from which they were injected into a time-of-flight mass analyzer, consisting of nine electrodes (four electrostatic mirror electrodes on each side of a grounded drift tube electrode) [35]. The ion bunches underwent around 600 turns between the electrostatic mirrors to increase the flight path, which increased the mass resolution to nearly 300 000 FWHM. After a predetermined number of turns, the potential of the second mirror was lowered and the ions were impinged on a MagneTOF detector to record the time-of-flight spectrum. A mass range selector (MRS) [36] in the MR-TOF-MS analyzer, comprised of two pairs of deflecting electrodes at the center of the central drift tube, was employed to ensure an unambiguous mass spectrum.

The Cr yield at the MR-TOF-MS dropped with increasing neutron number from $\approx 10^3$ pps for $^{59,61}\text{Cr}$ to < 1 pps for $^{64-65}\text{Cr}$, and is shown in Table 1. Sufficient statistics for each mass allowed for the peak identification, where lower yield isotopes were collected for longer time. The beam contained $^{27}\text{Co}^+$, $^{28}\text{Ni}^+$ and $^{31}\text{Ga}^+$ and doubly charged $^{50}\text{Sn}^{2+}$, $^{51}\text{Sb}^{2+}$, $^{54}\text{Xe}^{2+}$ and $^{56}\text{Ba}^{2+}$ atoms. Dominant diatomic oxides and fluorides present were TiO^+ , CaF^+ , and ScO^+ as seen in Fig. 2. Verification of the $^{59,61-65}\text{Cr}$ mass peaks was performed by blocking one step of the resonant ionization laser. In this situation, the Cr intensity reduced by a factor of 2–7 for the $^{59,61-65}\text{Cr}$ isotopes. Fig. 2 shows the drop in intensity of the ^{64}Cr peak with blocked lasers, while the intensity of other peaks remained constant. For ^{65}Cr , further investigation was required for the mass identification due to the lower statistics and a smaller change in the signal intensity with and without the resonant laser ionization. A reduction in laser enhancement has commonly been observed at ISAC for the most short-lived isotopes.

To validate the presence of ^{65}Cr , we performed a storage analysis measurement where the ion bunches were stored for varying times in the internal RFQ beam line of the MR-TOF-MS before transporting them to the mass analyzer [37]. These storage times were chosen with respect to ^{65}Cr 's half-life of 28 ms. From Fig. 3, it can be seen that the intensities of ^{65}Cr dropped while the intensities of long-lived ^{65}Co and ^{65}Ga stayed constant. A half-life of

Table 1

Mass excess values (in keV) determined in this work in comparison to previous works are shown for $^{59,61-65}\text{Cr}$ masses. Values from the ISOLTRAP [15] and the NSCL TOF-B ρ measurements [45,46] were taken for comparison with our results as well as for the reference/calibrant ions. We also list the approximate yield at the ISAC yield station and the total counts in MR-TOF for this measurement.

Isotopes	Yield (pps)	Counts	Mass calibrant	Mass excess (keV)		
				This work	Ref. [15]	Refs. [45,46]
^{59}Cr	17000	39000	^{59}Co	-48113(7)	-48115.9(0.7)	-48540(440)
^{61}Cr	–	300	$^{45}\text{Sc}^{16}\text{O}$	-42497(14)	-42496.5(1.8)	-43080(510)
^{62}Cr	850	170	$^{30}\text{Si}^{32}\text{S}$	-40855(19)	-40852.6(3.5)	-40890(490)
^{63}Cr	50	190	$^{44}\text{Ca}^{19}\text{F}$	-36204(18)	-36178(73)	-35940(430)
^{64}Cr	1	170	$^{48}\text{Sc}^{16}\text{O}$	-33573(26)		-33640(300)
^{65}Cr	0.3	140	$^{46}\text{Ca}^{19}\text{F}$	-28208(45)		-27280(780)

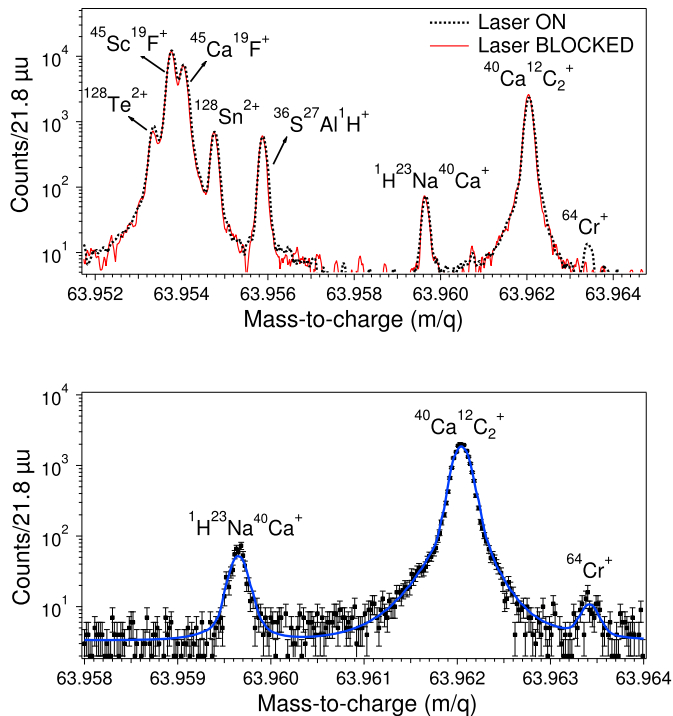


Fig. 2. (Top) Laser on (black dashed) versus blocked (red solid) spectra for $^{64}\text{Cr}^+$ shows a clear drop in ion counts when the laser was blocked and (Bottom) A zoomed spectra with error bars added shows the hyper-EMG fitting for $^{64}\text{Cr}^+$.

23(12) ms could be determined for ^{65}Cr which is consistent with the literature value of 27.5 (2.1) ms, further validating our assignment of ^{65}Cr .

The recorded TOF spectra were converted to the mass spectra using a calibration function

$$m/q = c(t - t_0)^2. \quad (1)$$

Here, m/q is the mass-to-charge ratio, c and t_0 are the calibration parameters, and t is the time of flight between injection into the analyzer and detection. The parameter t_0 is a small offset in timing caused by electronic delays and was determined from the time of flight of $^{39,41}\text{K}$ peaks undergoing only a time-focus shift turn [33]. It amounted to 209.2(5) ns. Parameter c was derived for each mass peak from a well-known reference ion. A time-resolved calibration (TRC) [38] was performed to correct for any time-dependent drifts arising from power supply instabilities and temperature fluctuations using the mass data acquisition (MAC) software package [39]. The dominant CaF^+ and TiO^+ ions were chosen as the calibration species for the TRC of $^{59}\text{Cr}^+$, $^{61}\text{Cr}^+$ and $^{62}\text{Cr}^+$ – $^{64}\text{Cr}^+$ masses, respectively. For $^{65}\text{Cr}^+$, $^{65}\text{Cu}^+$ was used as a reference for TRC. To determine the peak centroids, a hyper-EMG

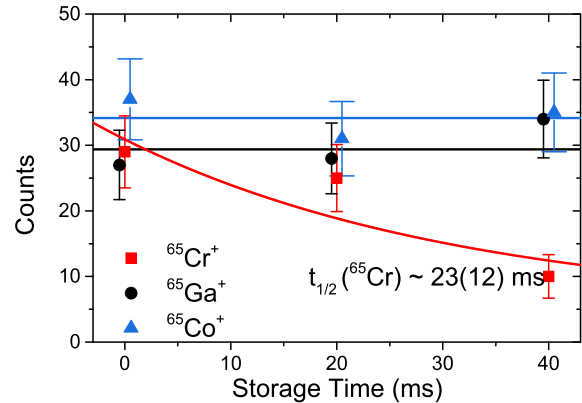


Fig. 3. Number of ions as a function of storage time in the MRTOF RFQ trap for $^{65}\text{Cr}^+$, $^{65}\text{Ga}^+$, and $^{65}\text{Co}^+$. A half-life of 23 ± 12 ms was obtained for ^{65}Cr compared to the reported NUBASE value of 27.5 ± 2.1 ms. The $^{65}\text{Cr}^+$ counts drops nearly exponentially while the $^{65}\text{Ga}^+$ and $^{65}\text{Co}^+$ counts are constant.

function [40] was fitted using the `emgfit` Python wrapper [41]. The hyper-EMG function particularly excels in fitting overlapping peaks such as the case of $^{64}\text{Cr}^+$ as can be seen in Fig. 2 [42]. The uncertainty in the determined mass values is a combination of the fitting uncertainty, AME uncertainty of the reference/calibrant ion, and a systematic uncertainty $\delta m/m$ of 1×10^{-7} [43,44]. On average, there is less than one ion per cycle in the MR-TOF. Therefore, the systematic shifts due to ion-ion interaction during this beam time were negligible. The weighted mean of the deviation of all identified species in the spectra, both atomic and molecular, from AME2020 masses was at the keV level, validating our assigned uncertainty.

3. Results and discussions

Table 1 lists the mass excess values evaluated in this work as well as comparisons with the previous measurements [15,45,46]. The recent AME2020 [47] evaluation includes the measurements from [15]. The TOF-B ρ measurements for ^{65}Cr reported in [45,46] was replaced in the AME2020 evaluation by an extrapolated value judged to be more accurate. This highlights the need for not only precise, but also accurate measurements. Here, mass excess (ME) is defined as, $ME(N, Z) = m_a(N, Z) - Am_u$, where m_a is the measured atomic mass and $m_u = 1 \text{ u} = 9.314940954(57) \times 10^8 \text{ eV}/c^2$. The reference ions strongest in statistics were chosen as calibrants for the mass determination and are listed for each chromium mass in Table 1.

Based on the new mass values we calculate the two-neutron separation energies S_{2n} , shown in Fig. 4, defined by Eqn. (2) for Cr ($Z=24$) to Ni ($Z=28$). Here $ME(N, Z)$ is the mass excess of an isotope with N neutrons and Z protons, M_n is the neutron mass excess.

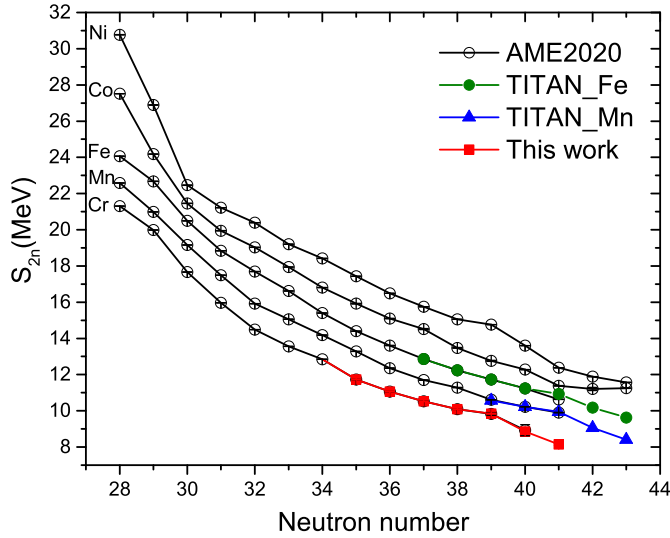


Fig. 4. Two-neutron separation energy (in MeV) for Ni ($Z=28$) through Cr ($Z=24$) is shown including the comparisons with AME2020 [47]. For Fe and Mn, recent TITAN measurements are also shown [48,23].

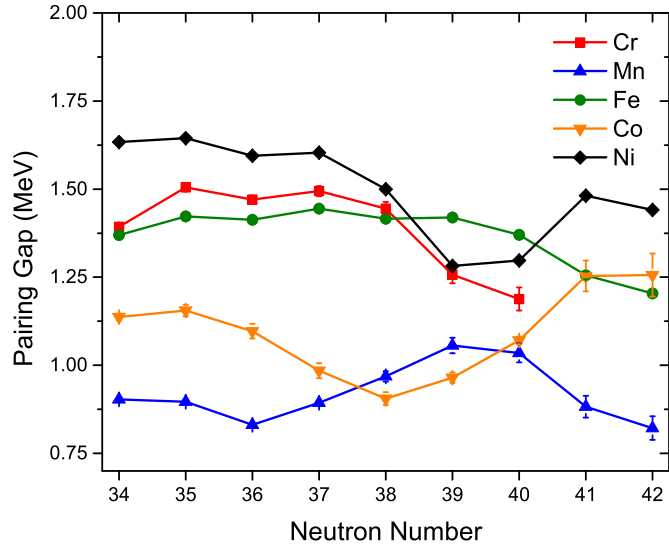


Fig. 5. Pairing gap energies along the $N=40$ IOI for Cr ($Z=24$) through Ni ($Z=28$) chain.

$$S_{2n}(N, Z) = ME(N-2, Z) - ME(N, Z) + 2M_n \quad (2)$$

The S_{2n} trend near the well-known shell-closure at $N=28$ is shown for comparison to the signatures at the $N=40$ region.

Our results agree with and extend beyond Mougeot *et al.*'s precise measurements of $^{59-63}\text{Cr}$ [15]. Their S_{2n} trend shows that unlike a sudden onset of deformation towards $N=40$ [45,49,50], an upward curvature in S_{2n} exists for the Cr chain up to $N=39$, which is interpreted as a gradual onset of collectivity in the ground-state of neutron-rich Cr isotopes similar to the neighboring Mn and Fe chains. Our extended measurements for $^{64,65}\text{Cr}$ isotopes show that the S_{2n} values do not follow this upward trend when approaching $N=40$. This also contradicts the similarity in the S_{2n} of Cr and Mn chain past ^{63}Cr ($N=39$).

In order to better understand the nature of the deformation in the Cr isotopes across $N=40$, Fig. 5 shows the pairing gap energies for Cr ($Z=24$) through Ni ($Z=28$), defined as

$$P_n(N, Z) = \frac{(-1)^{N+1}}{4} (S_n(Z, N+1) - S_n(Z, N-1)) \quad (3)$$

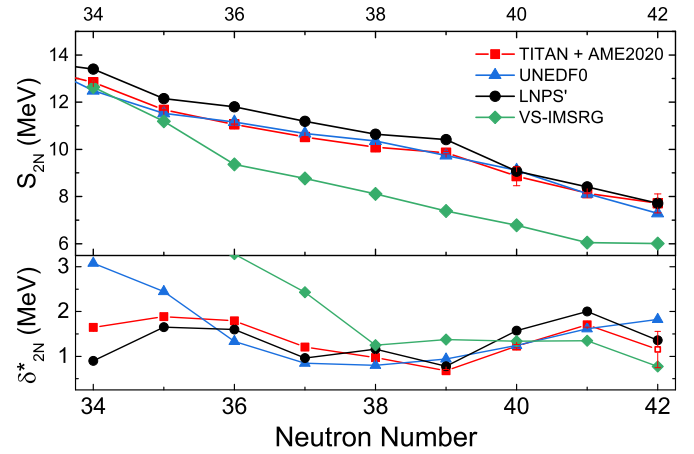


Fig. 6. Comparison of S_{2n} values (top) and δS_{2n} values (bottom) from VS-IMSRG($pf_{5/2}g_{9/2}d_{5/2}$), LNPS' and UNEDF0 theories with the TITAN results is shown.

$$-2S_n(Z, N) + S_n(Z, N-1)). \quad (3)$$

The pairing-gap energies in Cr show a nearly constant behavior until $N=37$, but then drops rapidly approaching $N=39$, which further points towards a more rapid change in correlation effects in Cr towards $N=40$. Interestingly, the Cr chain seems to tail the behavior seen in the Ni chain, whereas the in-between Mn chain shows a maximum pairing-gap energy at $N=39$. In Fe the constant pairing-gap energy region expands beyond $N=39$, but drops to the energy observed near the minimum in Ni only at $N=42$, and in Co a reduction occurs already past $N=35$. Similar discussions have been made by [18] and have indicated the delicate interplay between quadrupole deformation and pairing correlations.

To shine more light on the behavior observed in the Cr chain, we performed theoretical calculations using different approaches, as shown in Fig. 6. In addition to S_{2n} we show the two-neutron shell gap parameter, δ_{2n}^* in MeV defined by

$$\delta_{2n}^*(N, Z) = S_{2n}(N-2, Z) - S_{2n}(N, Z). \quad (4)$$

As seen in the figure, the decrease in the magnitude of S_{2n} agrees with the results from the mean-field calculations of the odd-even and even-even Cr isotopes from the UNEDF0 theory [25]. However, the δ_{2n}^* trend does not agree with the UNEDF0 theory. Both our S_{2n} and δ_{2n}^* trends match quite well with the LNPS' calculations, a modified version of LNPS [45] with 30 keV more attractive global monopole term [15]. Previous results from LNPS calculations [15,45,51] that include a valence space based on a ^{48}Ca core, a full pf -shell for protons and the neutron $pf_{5/2}g_{9/2}d_{5/2}$ orbitals, have shown a significant improvement over the GXPFA phenomenological calculations, and highlights the need to include the $g_{9/2}$ and $d_{5/2}$ neutron states to properly address the shell structure.

Fig. 6 also shows comparisons with a recently developed ab initio approach based on the VS-IMSRG, but which extends the calculations of the chromium chain with a mixed-parity valence space [26]. In this theory, an A -body unitary transformation is constructed to decouple the excitations involving the outside of a valence space [52–55]. From the computational point of view, the actual unitary transformation is constructed with the truncation to two-body level and induced many-body terms are neglected [referred to as the VS-IMSRG(2) approximation]. Following the framework outlined in Ref. [56], the energies of Cr isotopes are calculated starting from the 1.8/2.0 (EM) interaction [57], which provides the accurate ground-state energies compared to experiment up to at least the ^{132}Sn region [58,59], and in particular separation energies and shell gaps in this region [60,15,61,62,23].

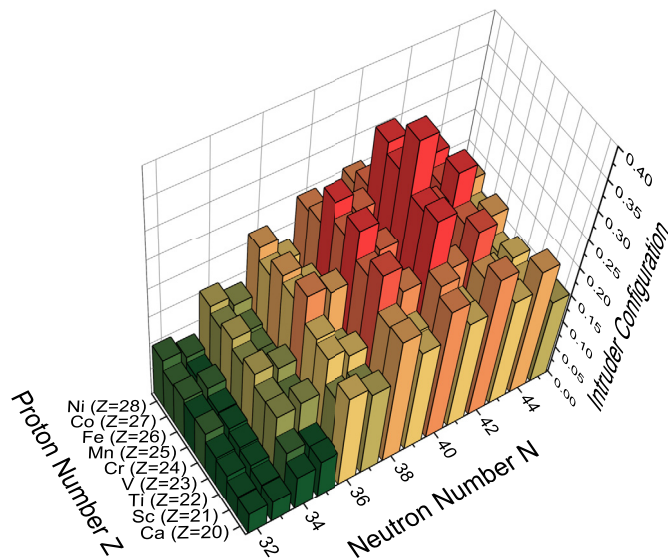


Fig. 7. The intruder contribution of the calculated ground-state wave function for the elements Ca ($Z=20$) through Ni ($Z=28$), computed by the VS-IMSRG(2) within the proton pf neutron $pf_{5/2}g_{9/2}$ valence space.

In this work, starting from the $\hbar\omega = 16$ MeV harmonic oscillator basis, our calculations are performed in the 15 major shell space to derive the effective Hamiltonian in the proton pf and neutron $pf_{5/2}g_{9/2}d_{5/2}$ valence space above ^{48}Ca core. Note that the neutron $d_{5/2}$ orbital is added to the valence space here, in contrast to the calculations in Ref. [15]. The three-body interaction matrix elements are restricted up to $E_{3\text{max}} = 16$, where $E_{3\text{max}}$ is defined as the sum of the three-body oscillator quanta. The center-of-mass Hamiltonian coefficient $\beta = 3$ is used in the following discussion and we observed that the β -dependence is negligibly small. For $N > 35$, the calculated S_{2n} are lower than the experiment, which was already observed in Ref. [15]. The discrepancy is attributed to the many-body correlations beyond the VS-IMSRG(2) approximation, implying the enhancement of the collectivity in $N > 35$.

It should be noted that the VS-IMSRG results systematically overestimate the excitation energies, while the trend of the experiment is well reproduced as shown in earlier works [26,63]. While too strong for $N < 38$, the VS-IMSRG δ_{2n}^* results follow the experimental trends in the IOI region well, as shown in Fig. 6, and thus we expect that the underlying physics is mostly captured through the VS-IMSRG(2) approximation. Nevertheless, since collectivity is an inherently many-body effect, we expect further improvement when advancing to the IMSRG(3) truncation for such calculations. Indeed implementation of IMSRG(3) has already been carried out in the single-reference formulation of the IMSRG for closed-shell systems [64], and first results for the VS-IMSRG are currently in preparation.

To further examine the extend of the $N=40$ IOI in the neighboring elements, we expand the VS-IMSRG calculations to cover the full region between Ca and Ni. In Fig. 7, the contributions of intruder configuration for Cr and neighboring elements are visualized using the calculated ground-state wave function from the VS-IMSRG within the proton pf and neutron $pf_{5/2}g_{9/2}$ valence space above ^{48}Ca . As seen in Fig. 7, towards $N=40$, the intruder configuration increases in the Cr ground states, a sign of IOI behavior at $N=40$ [51]. Also, the number of neutrons across the gap is maximized at $N=40$, consistent with the LNPS calculations [51].

This is similar to the trend in the $f_{7/2}$ and $p_{3/2}$ orbitals for ^{32}Mg [13,26]. Additionally, it is seen that the intruder state configuration is strongest for Cr compared to the neighboring nuclei, such as Mn, Fe and Co, shown in Fig. 7, implying that ^{64}Cr is the pinnacle of the $N=40$ IOI. The next strong contribution is seen for

Mn and Fe, with a similar trend where the intruder contribution is the strongest at $N=40$ followed by $N=42$. For Fe, this result is in agreement with the maximum observed quadrupole deformation between ^{66}Fe and ^{68}Fe (i.e. $N = 40$ and $N = 42$) from the mean-field calculations [23]. Another recent work on Mn has shown a high pairing gap approaching $N=40$ attributed to neutron occupying higher lying orbitals [48]. These results are in line with the results from LNPS calculations [51] that show the onset of deformation at $N=40$ in the Fe chain and at $N=38$ in Cr isotopes.

4. Conclusion and discussion

Our results reduce the uncertainties of the mass measurements for $^{63-65}\text{Cr}$ masses. Moreover, this presents the first high-precision direct mass measurements of $^{64,65}\text{Cr}$. Our results provide compelling evidence for maximal collectivity at ^{64}Cr centering it in an island of inversion around $N=40$. Comparison of our results with global mass-models and the ab-initio VS-IMSRG calculations indicates the dominance of the intruder configurations for ^{64}Cr , and shows the overall trend of collectivity in the region. The precise data provides important constraints to guide the ongoing development of ab-initio approaches to nuclear structure. High precision mass measurements beyond $N=41$ would be required to more fully probe the $N=40$ island of inversion. Advancement in the ab initio theory in this region will be significant in illuminating the nuclear shell structure for the $Z = 24$ nuclei.

Declaration of competing interest

The authors declare that they have no known competing financial interests or personal relationships that could have appeared to influence the work reported in this paper.

Acknowledgement

The authors would like to thank M. Good for his continual support, J. Lassen and the TRILIS group for their help with setting up the Cr lasers scheme for signal optimization, and S. R. Stroberg for the `imsrg++` code [65] used to perform these calculations. The shell-model diagonalization of VS-IMSRG calculations were done with the `KSHELL` code [66]. This work was supported by the Natural Sciences and Engineering Research Council (NSERC) of Canada under grants SAPIN-2018-00027 and RGPAS-2018-522453, by the National Research Council (NRC) of Canada through TRIUMF, by the UK Science and Technology Facilities Council STFC Grant No: ST/V001051/1, and by the Deutsche Forschungsgemeinschaft (DFG, German Research Foundation) – Project-ID 279384907 – SFB 1245. Computations were performed with an allocation of computing resources on Cedar at WestGrid and Compute Canada, and on the Oak Cluster at TRIUMF managed by the University of British Columbia department of Advanced Research Computing (ARC). We also thank K. Sieja for providing the LNPS' results.

References

- [1] J. Dilling, K. Blaum, M. Brodeur, S. Eliseev, Penning-trap mass measurements in atomic and nuclear physics, *Annu. Rev. Nucl. Part. Sci.* 68 (2018) 45–74, <https://doi.org/10.1146/annurev-nucl-102711-094939>.
- [2] D. Warner, Not-so-magic numbers, *Nature* 430 (2004) 517–519, <https://doi.org/10.1038/430517a>.
- [3] O. Sorlin, M.-G. Porquet, Nuclear magic numbers: new features far from stability, *Prog. Part. Nucl. Phys.* 61 (2) (2008) 602–673, <https://doi.org/10.1016/j.pnpnp.2008.05.001>.
- [4] D. Steppenbeck, S. Takeuchi, N. Aoi, P. Doornenbal, M. Matsushita, H. Wang, H. Baba, N. Fukuda, S. Go, M. Honma, J. Lee, K. Matsui, S. Michimasa, T. Motobayashi, D. Nishimura, T. Otsuka, H. Sakurai, Y. Shiga, P. Söderström, T. Sumikama, H. Suzuki, R. Taniuchi, Y. Utsuno, J.J. Valiente-Dobón, K. Yoneda, Evidence for a new nuclear ‘magic number’ from the level structure of ^{54}Ca , *Nature* 502 (7470) (2013) 207–210, <https://doi.org/10.1038/nature12522>.

- [5] F. Wienholtz, D. Beck, K. Blaum, C. Borgmann, M. Breitenfeldt, R.B. Cakirli, S. George, F. Herfurth, J.D. Holt, M. Kowalska, S. Kreim, D. Lunney, V. Manea, J. Menéndez, D. Neidherr, M. Rosenbusch, L. Schweikhard, A. Schwenk, J. Simonis, J. Stanja, R.N. Wolf, K. Zuber, Masses of exotic calcium isotopes pin down nuclear forces, *Nature* 498 (7454) (2013) 346–349, <https://doi.org/10.1038/nature12226>.
- [6] M. Bernas, P. Dessagne, M. Langevin, J. Payet, F. Pougheon, P. Roussel, Magic features of ^{68}Ni , *Phys. Lett. B* 113 (4) (1982) 279–282, [https://doi.org/10.1016/0370-2693\(82\)90039-9](https://doi.org/10.1016/0370-2693(82)90039-9).
- [7] C. Thibault, R. Klapisch, C. Rigaud, A.M. Poskanzer, R. Prieels, L. Lessard, W. Reisdorf, Direct measurement of the masses of ^{11}Li and $^{26-32}\text{Na}$ with an on-line mass spectrometer, *Phys. Rev. C* 12 (1975) 644–657, <https://doi.org/10.1103/PhysRevC.12.644>.
- [8] F. Sarazin, H. Savajols, W. Mittig, F. Nowacki, N.A. Orr, Z. Ren, P. Roussel-Chomaz, G. Auger, D. Baiborodin, A.V. Belozyorov, C. Borcea, E. Caurier, Z. Dlouhý, A. Gillibert, A.S. Lalleman, M. Lewitowicz, S.M. Lukyanov, F. de Oliveira, Y.E. Penionzhkevich, D. Ridikas, H. Sakurai, O. Tarasov, A. de Vismes, Shape coexistence and the $N = 28$ shell closure far from stability, *Phys. Rev. Lett.* 84 (2000) 5062–5065, <https://doi.org/10.1103/PhysRevLett.84.5062>.
- [9] O. Sorlin, M.-G. Porquet, Evolution of then = 28 shell closure: a test bench for nuclear forces, *Phys. Scr. T* 152 (2013) 014003, <https://doi.org/10.1088/0031-8949/2013/t152/014003>.
- [10] A. Gade, R.V.F. Janssens, D. Bazin, P. Farris, A.M. Hill, S.M. Lenzi, J. Li, D. Little, B. Longfellow, F. Nowacki, A. Poves, D. Rhodes, J.A. Tostevin, D. Weisshaar, In-beam γ -ray spectroscopy of $^{62,64}\text{Cr}$, *Phys. Rev. C* 103 (2021) 014314, <https://doi.org/10.1103/PhysRevC.103.014314>.
- [11] A. Gade, R.V.F. Janssens, T. Baugher, D. Bazin, B.A. Brown, M.P. Carpenter, C.J. Chiara, S.J. Deacon, A.N. Freeman, G.F. Grinyer, C.R. Hoffman, B.P. Kay, F.G. Kondev, T. Lauritsen, S. McDaniel, K. Meierbachtol, A. Ratkiewicz, S.R. Stroberg, K.A. Walsh, D. Weisshaar, R. Winkler, S. Zhu, Collectivity at $n = 40$ in neutron-rich ^{64}Cr , *Phys. Rev. C* 81 (2010) 051304, <https://doi.org/10.1103/PhysRevC.81.051304>.
- [12] S. Michimasa, M. Kobayashi, Y. Kiyokawa, S. Ota, R. Yokoyama, D. Nishimura, D.S. Ahn, H. Baba, G.P.A. Berg, M. Dozono, N. Fukuda, T. Furuno, E. Ideguchi, N. Inabe, T. Kawabata, S. Kawase, K. Kisanori, K. Kobayashi, T. Kubo, Y. Kubota, C.S. Lee, M. Matsushita, H. Miya, A. Mizukami, H. Nagakura, H. Oikawa, H. Sakai, Y. Shimizu, A. Stolz, H. Suzuki, M. Takaki, H. Takeda, S. Takeuchi, H. Tokieda, T. Uesaka, K. Yako, Y. Yamaguchi, Y. Yanagisawa, K. Yoshida, S. Shimoura, Mapping of a new deformation region around ^{62}Ti , *Phys. Rev. Lett.* 125 (2020) 122501, <https://doi.org/10.1103/PhysRevLett.125.122501>.
- [13] J. Ljungvall, A. Görgen, A. Obertelli, W. Kortén, E. Clément, G. de France, A. Bürger, J.-P. Delaroche, A. Dewald, A. Gadea, L. Gaudefroy, M. Girod, M. Hackstein, J. Libert, D. Mengoni, F. Nowacki, T. Pissulla, A. Poves, F. Recchia, M. Rejmund, W. Rother, E. Sahin, C. Schmitt, A. Shrivastava, K. Sieja, J.J. Valiente-Dobón, K.O. Zell, M. Zielińska, Onset of collectivity in neutron-rich fer isotopes: toward a new island of inversion?, *Phys. Rev. C* 81 (2010) 061301, <https://doi.org/10.1103/PhysRevC.81.061301>.
- [14] T. Baugher, A. Gade, R.V.F. Janssens, S.M. Lenzi, D. Bazin, B.A. Brown, M.P. Carpenter, A.N. Deacon, S.J. Freeman, T. Glasmacher, G.F. Grinyer, F.G. Kondev, S. McDaniel, A. Poves, A. Ratkiewicz, E.A. McCutchan, D.K. Sharp, I. Stefanescu, K.A. Walsh, D. Weisshaar, S. Zhu, Intermediate-energy Coulomb excitation of $^{58,60,62}\text{Cr}$: the onset of collectivity toward $n = 40$, *Phys. Rev. C* 86 (2012) 011305, <https://doi.org/10.1103/PhysRevC.86.011305>.
- [15] M. Mougéot, D. Atanasov, K. Blaum, K. Chrysalidis, T.D. Goodacre, D. Fedorov, V. Fedosseev, S. George, F. Herfurth, J.D. Holt, D. Lunney, V. Manea, B. Marsh, D. Neidherr, M. Rosenbusch, S. Rothe, L. Schweikhard, A. Schwenk, C. Seiffert, J. Simonis, S.R. Stroberg, A. Welker, F. Wienholtz, R.N. Wolf, K. Zuber, Precision mass measurements of $^{58-63}\text{Cr}$: nuclear collectivity towards the $n = 40$ island of inversion, *Phys. Rev. Lett.* 120 (2018) 232501, <https://doi.org/10.1103/PhysRevLett.120.232501>.
- [16] H.L. Crawford, R.M. Clark, P. Fallon, A.O. Macchiavelli, T. Baugher, D. Bazin, C.W. Beausang, J.S. Berryman, D.L. Bleuel, C.M. Campbell, M. Cromaz, G. de Angelis, A. Gade, R.O. Hughes, I.Y. Lee, S.M. Lenzi, F. Nowacki, S. Paschalis, M. Petri, A. Poves, A. Ratkiewicz, T.J. Ross, E. Sahin, D. Weisshaar, K. Wimmer, R. Winkler, Quadrupole collectivity in neutron-rich Fe and Cr isotopes, *Phys. Rev. Lett.* 110 (2013) 242701, <https://doi.org/10.1103/PhysRevLett.110.242701>.
- [17] T. Braunroth, A. Dewald, H. Iwasaki, S.M. Lenzi, M. Albers, V.M. Bader, T. Baugher, T. Baumann, D. Bazin, J.S. Berryman, C. Fransen, A. Gade, T. Ginter, A. Gottardo, M. Hackstein, J. Jolie, A. Lemasson, J. Litzinger, S. Lunardi, T. Marchi, V. Modamio, C. Morse, D.R. Napoli, A. Nichols, F. Recchia, S.R. Stroberg, R. Wadsworth, D. Weisshaar, K. Whitmore, K. Wimmer, Reduced transition strengths of low-lying yrast states in chromium isotopes in the vicinity of $n = 40$, *Phys. Rev. C* 92 (2015) 034306, <https://doi.org/10.1103/PhysRevC.92.034306>.
- [18] C. Santamaria, C. Louchart, A. Obertelli, V. Werner, P. Doornenbal, F. Nowacki, G. Authélet, H. Baba, D. Calvet, F. Château, A. Corsi, A. Delbart, J.-M. Gellera, A. Gillibert, T. Isobe, V. Lapoux, M. Matsushita, S. Momiyama, T. Motobayashi, M. Niikura, H. Otsu, C. Péron, A. Peyaud, E.C. Pollacco, J.-Y. Rousseff, H. Sakurai, M. Sasano, Y. Shiga, Y.S. Takeuchi, R. Taniuchi, T. Uesaka, H. Wang, K. Yoneda, F. Browne, L.X. Chung, Z. Dombradi, S. Franchoo, F. Giacoppo, A. Gottardo, K. Hadynska-Klek, Z. Korkulu, S. Koyama, Y. Kubota, J. Lee, M. Lettmann, R. Lozeva, K. Matsui, T. Miyazaki, S. Nishimura, L. Olivier, S. Ota, Z. Patel, N. Pietralla, E. Sahin, C. Shand, P.-A. Söderström, I. Stefan, D. Steppenbeck, T. Sumikama, D. Suzuki, Z. Vajta, J. Wu, Z. Xu, Extension of the $n = 40$ island of inversion towards $n = 50$: spectroscopy of ^{66}Cr , $^{70,72}\text{Fe}$, *Phys. Rev. Lett.* 115 (2015) 192501, <https://doi.org/10.1103/PhysRevLett.115.192501>.
- [19] F. Nowacki, A. Obertelli, A. Poves, The neutron-rich edge of the nuclear landscape: experiment and theory, *Prog. Part. Nucl. Phys.* 120 (2021) 103866, <https://doi.org/10.1016/j.pnpnp.2021.103866>.
- [20] F. Nowacki, A. Poves, E. Caurier, B. Bounthong, Shape coexistence in ^{78}Ni as the portal to the fifth island of inversion, *Phys. Rev. Lett.* 117 (2016) 272501, <https://doi.org/10.1103/PhysRevLett.117.272501>.
- [21] A.A. Kwiatkowski, C. Andreoiu, J.C. Bale, A. Chaudhuri, U. Chowdhury, S. Malbrunot-Ettenauer, A.T. Gallant, A. Grossheim, G. Gwinner, A. Lennarz, T.D. Macdonald, T.J.M. Rauch, B.E. Schultz, S. Seeraji, M.C. Simon, V.V. Simon, D. Lunney, A. Poves, J. Dilling, Observation of a crossover of 5_{2n}^+ in the island of inversion from precision mass spectrometry, *Phys. Rev. C* 92 (2015) 061301, <https://doi.org/10.1103/PhysRevC.92.061301>.
- [22] T. Otsuka, T. Suzuki, R. Fujimoto, H. Grawe, Y. Akaishi, Evolution of nuclear shells due to the tensor force, *Phys. Rev. Lett.* 95 (2005) 232502, <https://doi.org/10.1103/PhysRevLett.95.232502>.
- [23] W.S. Porter, B. Ashrafkhani, J. Bergmann, C. Brown, T. Brunner, J.D. Cardona, D. Curien, I. Dedes, T. Dickel, J. Dudek, E. Dunling, G. Gwinner, Z. Hockenbery, J.D. Holt, C. Hornung, C. Izzo, A. Jacobs, A. Javaji, B. Kootte, G. Kriepkó-Koncz, E.M. Lykiardopoulou, T. Miyagi, I. Mukul, T. Murboeck, W.R. Plaß, M.P. Reiter, J. Ringuette, C. Scheidenberger, R. Silwal, H.L. Walls, C. Wang, Y. Wang, J. Yang, J. Dilling, A.A. Kwiatkowski, Mapping the northern shore of the $n = 40$ island of inversion: precision mass measurements of neutron-rich Fe isotopes, *Phys. Rev. C* (2022).
- [24] A. Poves, J. Retamosa, Onset of deformation at the $n=20$ neutron shell closure far from stability, *Phys. Lett. B (Netherlands)* 184 (4) (Feb 1987).
- [25] M. Kortelainen, T. Lesinski, J. Moré, W. Nazarewicz, J. Sarich, N. Schunck, M.V. Stoitsov, S. Wild, Nuclear energy density optimization, *Phys. Rev. C* 82 (2010) 024313, <https://doi.org/10.1103/PhysRevC.82.024313>.
- [26] T. Miyagi, S.R. Stroberg, J.D. Holt, N. Shimizu, Ab initio multishell valence-space hamiltonians and the island of inversion, *Phys. Rev. C* 102 (2020) 034320, <https://doi.org/10.1103/PhysRevC.102.034320>.
- [27] C. Jesch, T. Dickel, W.R. Plaß, D. Short, S. Ayet San Andres, J. Dilling, H. Geissel, F. Greiner, J. Lang, K.G. Leach, W. Lippert, C. Scheidenberger, M.I. Yavor, The mrt-of-ms isobar separator for the titan facility at triumpf, *Hyperfine Interact.* 235 (2015) 97–106, <https://doi.org/10.1007/s10751-015-1184-2>.
- [28] G.C. Ball, G. Hackman, R. Krücken, The triumpf isac facility: two decades of discovery with rare isotope beams, *Phys. Scr.* 91 (2016) 93002, <https://doi.org/10.1088/0031-8949/91/9/093002>.
- [29] J. Lassen, R. Li, S. Raeder, X. Zhao, T. Dekker, H. Heggen, P. Kunz, P.C.D. Levy, M. Mostanmand, A. Teigelhöfer, F. Ames, Current developments with triumpf's titanium-sapphire laser based resonance ionization laser ion source, *Hyperfine Interact.* 238 (2017) 33, <https://doi.org/10.1007/s10751-017-1407-9>.
- [30] Y. Kudryavtsev, R. Ferrer, M. Huysse, P. Van den Bergh, P. Van Duppen, L. Vermeeren, Two-step laser ionization schemes for in-gas laser ionization and spectroscopy of radioactive isotopes, *Rev. Sci. Instrum.* 85 (2) (2014) 02B915, <https://doi.org/10.1063/1.4850695>.
- [31] P. Bricault, R. Baartman, M. Dombbsky, A. Hurst, C. Mark, G. Stanford, P. Schmor, Triumpf-isac target station and mass separator commissioning, in: 5th International Conference on Radioactive Nuclear Beams, *Nucl. Phys. A* 701 (2002) 49–53, [https://doi.org/10.1016/S0375-9474\(01\)01546-9](https://doi.org/10.1016/S0375-9474(01)01546-9).
- [32] T. Brunner, M. Smith, M. Brodeur, S. Ettenauer, A. Gallant, V. Simon, A. Chaudhuri, A. Lapiere, E. Mané, R. Ringle, M. Simon, J. Vaz, P. Delheij, M. Good, M. Pearson, J. Dilling, Titan's digital rfq ion beam cooler and buncher, operation and performance, *Nucl. Instrum. Methods Phys. Res., Sect. A, Accel. Spectrom. Detect. Assoc. Equip.* 676 (2012) 32–43, <https://doi.org/10.1016/j.nima.2012.02.004>.
- [33] M. Reiter, S.A.S. Andrés, J. Bergmann, T. Dickel, J. Dilling, A. Jacobs, A. Kwiatkowski, W. Plaß, C. Scheidenberger, D. Short, C. Will, C. Babcock, E. Dunling, A. Finlay, C. Hornung, C. Jesch, R. Klawitter, B. Kootte, D. Lascar, E. Leitschneider, T. Murböck, S. Paul, M. Yavor, Commissioning and performance of titan's multiple-reflection time-of-flight mass-spectrometer and isobar separator, *Nucl. Instrum. Methods Phys. Res., Sect. A, Accel. Spectrom. Detect. Assoc. Equip.* 1018 (2021) 165823, <https://doi.org/10.1016/j.nima.2021.165823>.
- [34] W.R. Plaß, T. Dickel, C. Scheidenberger, Multiple-reflection time-of-flight mass spectrometry, *Int. J. Mass Spectrom.* 349–350 (2013) 134–144, <https://doi.org/10.1016/j.ijms.2013.06.005>.
- [35] M.I. Yavor, W.R. Plaß, T. Dickel, H. Geissel, C. Scheidenberger, Ion-optical design of a high-performance multiple-reflection time-of-flight mass spectrometer and isobar separator, *Int. J. Mass Spectrom.* 381–382 (2015) 1–9, <https://doi.org/10.1016/j.ijms.2015.01.002>, <https://www.sciencedirect.com/science/article/pii/S1387380615000202>.
- [36] T. Dickel, W.P.A. Becker, U. Czok, H. Geissel, E. Haettner, C. Jesch, W. Kinsel, M. Petrick, C. Scheidenberger, A. Simon, M. Yavor, A high-performance multiple-reflection time-of-flight mass spectrometer and isobar separator for the research with exotic nuclei, *Nucl. Instrum. Methods Phys. Res., Sect. A, Accel.*

- Spectrom. Detect. Assoc. Equip. 777 (2015) 172–188, <https://doi.org/10.1016/j.nima.2014.12.094>.
- [37] I. Mukul, C. Andreoiu, M. Brodeur, T. Brunner, K. Dietrich, T. Dickel, I. Dillmann, E. Dunling, D. Fusco, G. Gwinner, C. Izzo, A. Jacobs, B. Kootte, Y. Lan, E. Leistschneider, M. Lykiardopoulou, S. Paul, M. Reiter, J. Tracy, A. Kwiatkowski, Measuring the half-life of n-rich ^{100}rb with the titan mr-tof-ms, *J. Phys. Conf. Ser.* 1643 (2020) 012057, <https://doi.org/10.1088/1742-6596/1643/1/012057>.
- [38] J. Ebert, Mass measurements of ^{238}u -projectile fragments for the first time with a multiple-reflection time-of-flight mass spectrometer, Ph.D. thesis, Justus-Liebig-Universität Giessen, 2016.
- [39] T. Dickel, W. Plaß, W. Lippert Wayne, J. Lang, I. Mikhail, H. Geissel, C. Scheidenberger, Isobar separation in a multiple-reflection time-of-flight mass spectrometer by mass-selective re-trapping, *J. Am. Soc. Mass Spectrom.* 28 (2017) 1079–1090, <https://doi.org/10.1007/s13361-017-1617-z>.
- [40] S. Purushothaman, S. Ayet San Andrés, J. Bergmann, T. Dickel, J. Ebert, H. Geissel, C. Hornung, W.R. Plaß, C. Rappold, C. Scheidenberger, Y.K. Tanaka, M.I. Yavor Hyper-emg, A new probability distribution function composed of exponentially modified gaussian distributions to analyze asymmetric peak shapes in high-resolution time-of-flight mass spectrometry, *Int. J. Mass Spectrom.* 421 (2017) 245–254, <https://doi.org/10.1016/j.ijms.2017.07.014>.
- [41] S.F. Paul, <https://pyypi.org/project/emgfit>.
- [42] S. Ayet San Andrés, C. Hornung, J. Ebert, W.R. Plaß, T. Dickel, H. Geissel, C. Scheidenberger, J. Bergmann, F. Greiner, E. Haettner, C. Jesch, W. Lippert, I. Mardor, I. Miskun, Z. Patyk, S. Pietri, A. Pihktelev, S. Purushothaman, M.P. Reiter, A.-K. Rink, H. Weick, M.I. Yavor, S. Bagchi, V. Charviakova, P. Constantin, M. Diwisch, A. Finlay, S. Kaur, R. Knöbel, J. Lang, B. Mei, I.D. Moore, J.-H. Otto, I. Pohjalainen, A. Prochazka, C. Rappold, M. Takechi, Y.K. Tanaka, J.S. Winfield, X. Xu, High-resolution, accurate multiple-reflection time-of-flight mass spectrometry for short-lived, exotic nuclei of a few events in their ground and low-lying isomeric states, *Phys. Rev. C* 99 (2019) 064313, <https://doi.org/10.1103/PhysRevC.99.064313>.
- [43] A. Jacobs, Collision induced dissociation and mass spectrometry with the titan multiple-reflection time-of-flight mass-spectrometer, M.Sc. thesis, University of British Columbia, 2019, <https://open.library.ubc.ca/collections/ubctheses/24/items/1.0380561>.
- [44] S.F. Paul, J. Bergmann, J.D. Cardona, K.A. Dietrich, E. Dunling, Z. Hockenbery, C. Hornung, C. Izzo, A. Jacobs, A. Javaji, B. Kootte, Y. Lan, E. Leistschneider, E.M. Lykiardopoulou, I. Mukul, T. Murböck, W.S. Porter, R. Silwal, M.B. Smith, J. Ringuette, T. Brunner, T. Dickel, I. Dillmann, G. Gwinner, M. MacCormick, M.P. Reiter, H. Schatz, N.A. Smirnova, J. Dilling, A.A. Kwiatkowski, Mass measurements of $^{60-63}\text{Ga}$ reduce x-ray burst model uncertainties and extend the evaluated $T = 1$ isobaric multiplet mass equation, *Phys. Rev. C* 104 (6) (2021) 065803, <https://doi.org/10.1103/PhysRevC.104.065803>.
- [45] Z. Meisel, S. George, S. Ahn, D. Bazin, B.A. Brown, J. Browne, J.F. Carpino, H. Chung, R.H. Cyburt, A. Estradé, M. Famiano, A. Gade, C. Langer, M. Matoš, W. Mittig, F. Montes, D.J. Morrissey, J. Pereira, H. Schatz, J. Schatz, M. Scott, D. Shapira, K. Sieja, K. Smith, J. Stevens, W. Tan, O. Tarasov, S. Towers, K. Wimmer, J.R. Winkelbauer, J. Yurkon, R.G.T. Zegers, Time-of-flight mass measurements of neutron-rich chromium isotopes up to $n = 40$ and implications for the accreted neutron star crust, *Phys. Rev. C* 93 (2016) 035805, <https://doi.org/10.1103/PhysRevC.93.035805>.
- [46] Z. Meisel, S. George, S. Ahn, D. Bazin, B.A. Brown, J. Browne, J.F. Carpino, H. Chung, R.H. Cyburt, A. Estradé, M. Famiano, A. Gade, C. Langer, M. Matoš, W. Mittig, F. Montes, D.J. Morrissey, J. Pereira, H. Schatz, J. Schatz, M. Scott, D. Shapira, K. Smith, J. Stevens, W. Tan, O. Tarasov, S. Towers, K. Wimmer, J.R. Winkelbauer, J. Yurkon, R.G.T. Zegers, Nuclear mass measurements map the structure of atomic nuclei and accreting neutron stars, *Phys. Rev. C* 101 (2020) 052801, <https://doi.org/10.1103/PhysRevC.101.052801>.
- [47] W. Huang, M. Wang, F.G. Kondev, G. Audi, S. Naimi, The ame 2020 atomic mass evaluation (i). Evaluation of input data, and adjustment procedures, *Chin. Phys. C* 45 (3) (2021) 030002, <https://doi.org/10.1088/1674-1137/45/3/030002>.
- [48] A.T. Gallant, M.P. Reiter, C. Babcock, T. Dickel, E. Dunling, Z. Hockenbery, J.D. Holt, B. Kootte, R. Klawitter, Y. Lan, J. Lassen, E. Leistschneider, J. Menéndez, M. Vansteenkiste, M. Yavor, C. Andreoiu, I. Dillmann, G. Gwinner, R. Thompson, M.E. Wieser, A.A. Kwiatkowski, J. Dilling, Probing the $n = 40$ island of inversion through manganese masses, *Am. Phys. Soc.* (2021), submitted for publication.
- [49] S. Naimi, G. Audi, D. Beck, K. Blaum, C. Böhm, C. Borgmann, M. Breitenfeldt, S. George, F. Herfurth, A. Herlert, A. Kellerbauer, M. Kowalska, D. Lunney, E. Minaya Ramirez, D. Neidherr, M. Rosenbusch, L. Schweikhard, R.N. Wolf, K. Zuber, Surveying the $n = 40$ island of inversion with new manganese masses, *Phys. Rev. C* 86 (2012) 014325, <https://doi.org/10.1103/PhysRevC.86.014325>.
- [50] C. Babcock, H. Heylen, M. Bissell, K. Blaum, P. Campbell, B. Cheal, D. Fedorov, R. Garcia Ruiz, W. Geithner, W. Gins, T. Day Goodacre, L. Grob, M. Kowalska, S. Lenzi, B. Maass, S. Malbrunot-Ettenauer, B. Marsh, R. Neugart, G. Neyens, W. Nörtershäuser, T. Otsuka, R. Rossel, S. Rothe, R.S. 'anchez, Y. Tsunoda, C. Wraith, L. Xie, X. Yang, Quadrupole moments of odd- a ^{5363}mn : onset of collectivity towards $n=40$, *Phys. Lett. B* 760 (2016) 387–392, <https://doi.org/10.1016/j.physletb.2016.07.016>.
- [51] S.M. Lenzi, F. Nowacki, A. Poves, K. Sieja, Island of inversion around ^{64}cr , *Phys. Rev. C* 82 (5) (2010) 054301, <https://doi.org/10.1103/PhysRevC.82.054301>.
- [52] H. Hergert, S.K. Bogner, T.D. Morris, A. Schwenk, K. Tsukiyama, The in-medium similarity renormalization group: a novel ab initio method for nuclei, *Phys. Rep.* 621 (2016) 165, <https://doi.org/10.1016/j.physrep.2015.12.007>.
- [53] T.D. Morris, N.M. Parzuchowski, S.K. Bogner, Magnus expansion and in-medium similarity renormalization group, *Phys. Rev. C* 92 (2015) 034331, <https://doi.org/10.1103/PhysRevC.92.034331>.
- [54] S.K. Bogner, H. Hergert, J.D. Holt, A. Schwenk, S. Binder, A. Calci, J. Langhammer, R. Roth, Nonperturbative shell-model interactions from the in-medium similarity renormalization group, *Phys. Rev. Lett.* 113 (14) (2014) 142501, <https://doi.org/10.1103/PhysRevLett.113.142501>, arXiv:1402.1407.
- [55] S.R. Stroberg, H. Hergert, S.K. Bogner, J.D. Holt, Nonempirical interactions for the nuclear shell model: an update, *Annu. Rev. Nucl. Part. Sci.* 69 (1) (2019) 307–362, <https://doi.org/10.1146/annurev-nucl-101917-021120>, arXiv:1902.06154.
- [56] S.R. Stroberg, A. Calci, H. Hergert, J.D. Holt, S.K. Bogner, R. Roth, A. Schwenk, Nucleus-dependent valence-space approach to nuclear structure, *Phys. Rev. Lett.* 118 (2017) 032502, <https://doi.org/10.1103/PhysRevLett.118.032502>.
- [57] K. Hebeler, S.K. Bogner, R.J. Furnstahl, A. Nogga, A. Schwenk, Improved nuclear matter calculations from chiral low-momentum interactions, *Phys. Rev. C* 83 (3) (2011) 031301, <https://doi.org/10.1103/PhysRevC.83.031301>, arXiv:1012.3381.
- [58] S.R. Stroberg, J.D. Holt, A. Schwenk, J. Simonis, Ab initio limits of atomic nuclei, *Phys. Rev. Lett.* 126 (2) (2021) 022501, <https://doi.org/10.1103/PhysRevLett.126.022501>, arXiv:1905.10475.
- [59] T. Miyagi, S.R. Stroberg, P. Navrátil, K. Hebeler, J.D. Holt, Converged ab initio calculations of heavy nuclei, *Phys. Rev. C* 105 (1) (2022) 014302, <https://doi.org/10.1103/PhysRevC.105.014302>.
- [60] E. Leistschneider, et al., Dawning of the $N = 32$ shell closure seen through precision mass measurements of neutron-rich titanium isotopes, *Phys. Rev. Lett.* 120 (6) (2018) 062503, <https://doi.org/10.1103/PhysRevLett.120.062503>.
- [61] X. Xu, et al., Masses of neutron-rich $^{52-54}\text{Sc}$ and $^{54,56}\text{Ti}$ nuclides: the $N = 32$ subshell closure in scandium, *Phys. Rev. C* 99 (6) (2019) 064303, <https://doi.org/10.1103/PhysRevC.99.064303>.
- [62] E. Leistschneider, et al., Precision mass measurements of neutron-rich scandium isotopes refine the evolution of $N = 32$ and $N = 34$ shell closures, *Phys. Rev. Lett.* 126 (4) (2021) 042501, <https://doi.org/10.1103/PhysRevLett.126.042501>.
- [63] J. Simonis, S.R. Stroberg, K. Hebeler, J.D. Holt, A. Schwenk, Saturation with chiral interactions and consequences for finite nuclei, *Phys. Rev. C* 96 (1) (2017) 014303, <https://doi.org/10.1103/PhysRevC.96.014303>, arXiv:1704.02915.
- [64] M. Heinz, A. Tichai, J. Hoppe, K. Hebeler, A. Schwenk, In-medium similarity renormalization group with three-body operators, *Phys. Rev. C* 103 (4) (2021) 044318, <https://doi.org/10.1103/PhysRevC.103.044318>.
- [65] S.R. Stroberg, <https://github.com/ragnarstroberg/imsrg>.
- [66] N. Shimizu, T. Mizusaki, Y. Utsuno, Y. Tsunoda, Thick-restart block Lanczos method for large-scale shell-model calculations, *Comput. Phys. Commun.* 244 (2019) 372–384, <https://doi.org/10.1016/j.cpc.2019.06.011>, <https://linkinghub.elsevier.com/retrieve/pii/S0010465519301985>.